SANDIA REPORT
SAND2004–8085
Unlimited Release
Printed March 2004

Soot Properties and Species Measurements in a Two-Meter Diameter JP-8 Pool Fire: 2003 Test Series

Jeffrey J. Murphy and Christopher R. Shaddix

Prepared by
Sandia National Laboratories
Albuquerque, New Mexico 87185 and Livermore, California 94550

Sandia is a multiprogram laboratory operated by Sandia Corporation,
a Lockheed Martin Company, for the United States Department of Energy's
National Nuclear Security Administration under Contract DE-AC04-94AL85000.

Sandia National Laboratories

Issued by Sandia National Laboratories, operated for the United States Department of Energy by Sandia Corporation.

Available to DOE and DOE contractors from
U.S. Department of Energy
Office of Scientific and Technical Information
P.O. Box 62
Oak Ridge, TN 37831

Telephone: (865)576-8401
Facsimile: (865)576-5728
E-Mail: reports@adonis.osti.gov
Online ordering: http://www.doe.gov/bridge

Available to the public from
U.S. Department of Commerce
National Technical Information Service
5285 Port Royal Rd
Springfield, VA 22161

Telephone: (800)553-6847
Facsimile: (703)605-6900
E-Mail: orders@ntis.fedworld.gov
Online order: http://www.ntis.gov/help/ordermethods.asp?loc=7-4-0#online

SAND2004–8085
Unlimited Release
Printed March 2004

Soot Properties and Species Measurements in a Two-Meter Diameter JP-8 Pool Fire: 2003 Test Series

Jeffrey J. Murphy and Christopher R. Shaddix

Combustion Research Facility
Sandia National Laboratories
P.O. Box 969, Livermore, CA 94550

Abstract

A tunable diode laser absorption spectroscopy probe was used to measure in situ soot properties and species concentrations in a two-meter diameter JP-8 pool fire. Thirty-five tests were performed at the Lurance Canyon Burn Site operated by Sandia in Albuquerque, New Mexico. The axial profile of the fire was characterized with a series of tests with the probe located on the centerline at heights ranging from 0.5 m to 2.0 m in 0.25 m increments. The radial profile of the fire was characterized with a series of tests with the probe 1.0 m above the fuel surface at radial positions ranging from 0.0 m to 0.6 m, in 0.1 m increments. Experiments were also performed with variation of the air flow into the facility. Soot concentration was determined using a light extinction measurement based on the transmission of a solid-state red laser (635 nm) through the 3.7 cm long probe volume. Soot temperature and a second estimate of soot concentration were measured using two-color optical pyrometry at 850 nm and 1000 nm. The effective data rate for these measurements was 10 kHz. Finally, tunable diode laser absorption spectroscopy was used to estimate the concentrations of water vapor, acetylene, and methane. The results presented include the statistics, probability density functions, and spectral density functions of soot concentration, soot temperature, and approximate species concentrations at the different measurement locations throughout the fire.

Acknowledgements

The authors would like to thank Tom Blanchat and the crew at the Lurance Canyon Burn Site for providing the facilities and supporting the experiments detailed in this report. Doug Scott of Sandia was responsible for the design and fabrication of the custom lock-in amplifiers used for the TDL measurements. Gary Hubbard of Hubbard Associates wrote the data acquisition software.

Contents

List of Figures

List of Tables

This page intentionally left blank.

Nomenclature

a	line strength
B	molecular rotation constant
c	speed of light [m/s]
C_1	first radiation constant $= 3.741\,771 \times 10^{-16}$ W m^2
C_2	second radiation constant $= 1.438\,775 \times 10^{-2}$ m K
d	particle diameter [nm], or molecular state degeneracy
E	internal molecular energy [cm^{-1}]
f	arbitrary dependent variable
f_v	soot volume fraction [ppm]
h	constant
I	intensity [W/m^2]
J	rotational quantum number
k	Boltzmann's constant
K	dimensionless soot extinction coefficient $= k\lambda/f_v$
k	soot extinction coefficient [m^{-1}]
N	total number of independent variables, or molecular number density [kmol/m^3]
p	pressure [Pa]
Q	Partition function
s	path length [m]
S	spectral line strength []
T	temperature [K]
$\tilde{T}$	normalized temperature $= T/1000$ K
t_n	Student's t variable for n degrees of freedom
v	vibrational quantum number
V	voltage [V]
x	arbitrary independent variable

Greek symbols

Δf	indicates a difference between two values of f
ε	emissivity
λ	wavelength [nm]
ν_0	energy of molecular transition [cm^{-1}]
π	3.141 593...
σ	standard deviation, or line strength temperature dependence, or molecular rotational symmetry parameter
ω	energy for simple harmonic oscillator [cm^{-1}]

Subscripts

0	initial
a	absorption

b	blackbody
e	emission or extinction
i	index
j	index
ref	reference value
t	transmission
λ	spectral quantity

Introduction

This report describes a series of thirty-five tests where soot concentration, soot temperature, and species concentrations were measured as a function of position in a two-meter diameter pool fire. These experiments were performed in July of 2003 at Sandia's Lurance Canyon Burn Site near Albuquerque, New Mexico. The work is an extension of a previous study [1], performed in August 2002 in the same facility. The present study includes measurements of acetylene and methane in addition to water vapor, and characterizes both a radial profile and the axial profile of the fire. The measurements presented here supercede those presented in the previous study [1].

Description of Diagnostics

Soot Measurement

The visible laser absorption/soot emission diagnostic was the same as that used previously [1]; we repeat the description here for completeness. A 9 μm single-mode fiber is used to transport light to the probe volume for the transmission measurement. The laser light is collimated with a 4.6 mm aspherical lens and then projected across the probe volume. The light is then collected via a 5.5 mm diameter aspherical lens onto a 62.5 μm solid-core multimode fiber and transmitted back to the equipment trailer. The combination of the 9 μm delivery fiber and the 62.5 μm receiving fiber is insensitive to beam steering. The lenses are mounted behind the TDL Herriott cell mirrors (see page 14), and use centerline holes drilled through the mirrors for optical access to the probe volume.

The laser source is a directly modulated 635 nm diode laser. We impose a sinusoidal modulation at high frequency (50 kHz) and then use an analog lock-in amplifier with a time constant of 100 μs to provide a measurement of the transmitted laser power that is completely insensitive to thermal emission or any other light sources. The combination of the modulated laser and the narrow field of view of the fiber optic ensures that this is a true extinction measurement. A low-pass spectral filter is used to clean up the output of the diode laser and a laser-line notch filter further rejects any competing light sources incident upon the reference or signal diode detectors.

A dichroic beamsplitter is used at the output end of the receiving fiber to separate the near-infrared wavelengths from the transmission measurement laser signal. Silicon avalanche photodiodes (APDs), each with a 5 kHz bandwidth, 3 mm diameter active area, and thermoelectric cooler for temperature stabilization, are used to detect the thermal emission signals through near-IR bandpass filters. The transmissivity and emission data were recorded at approximately 89 kHz. During post-processing, the data were averaged to give an effective sample rate of 10 kHz.

The emission measurement was calibrated with a blackbody source (emissivity 0.97–0.98) overfilling the collection optics. The source was aimed into the head end of the probe with a silver mirror (reflectivity 0.98–0.99). A multi-point calibration was performed from

1220–1460 K using neutral density filters with a combined optical density of 1.5 (3.2% transmittance). The resulting effective emissivity of the source was 0.03.

The APDs continue to have a problem with 120 Hz noise. As a result, the power spectra of the emission measurements have strong peaks at 120 Hz and higher harmonics. At this point, the source of the noise is unknown.

Theory of the Soot Absorption / Emission Diagnostic

From the 635 nm transmissivity measurement, the soot extinction coefficient in the probe volume is determined:

$$k_{e,\lambda} \equiv \frac{K_{e,\lambda} f_{v,t}}{\lambda} = -\frac{1}{s} \ln\left(\frac{I_\lambda}{I_{\lambda,0}}\right) \tag{1}$$

Here, $I_\lambda / I_{\lambda,0}$ is the measured transmissivity and s is the path length. This equation is a version of the transmissivity function defined on page 233 of Brewster [2], and is strictly valid only for a homogeneous medium. As applied to our measurement, $k_{e,\lambda}$ is a mean extinction coefficient corresponding to a mean soot volume fraction, that is

$$k_{e,\lambda} = \frac{1}{s}\int_0^s k'_{e,\lambda}\,\mathrm{d}s' = \frac{K_{e,\lambda} f_{v,t}}{\lambda} = \frac{1}{\lambda s}\int_0^s K'_{e,\lambda} f'_{v,t}\,\mathrm{d}s' \tag{2}$$

Utilizing an estimate of the mean dimensionless spectral extinction coefficient $K_{e,\lambda}$, the mean soot volume fraction is determined from the measurement using

$$f_{v,t} = -\frac{\lambda}{K_{e,\lambda} s} \ln\left(\frac{I_\lambda}{I_{\lambda,0}}\right) \tag{3}$$

where λ is the laser wavelength.

Soot temperature is determined from soot emission intensity, which is in turn governed by Planck's black-body radiation law:

$$I_{b,\lambda}(T) = \frac{C_1/\pi}{\lambda^5 (\mathrm{e}^{C_2/\lambda T} - 1)} \tag{4}$$

Here, λ is the emission wavelength. After calibration with a reference source of emissivity $\varepsilon_{\mathrm{ref}}$ and temperature T_{ref}, the voltage output V_λ of the detector, which is proportional to the detected intensity, is

$$\frac{V_\lambda}{V_{\lambda,\mathrm{ref}}} = \frac{\varepsilon_\lambda}{\varepsilon_{\mathrm{ref}}} \frac{\mathrm{e}^{C_2/\lambda T_{\mathrm{ref}}} - 1}{\mathrm{e}^{C_2/\lambda T} - 1} \tag{5}$$

Emission is measured at two wavelengths, 850 nm and 1000 nm. Using the typical expression for emissivity due to soot, $\varepsilon_\lambda = (1 - \mathrm{e}^{-K_{a,\lambda} f_{v,e} s/\lambda})$ (see Ref. 3), we have two equations and two unknowns that can be solved for temperature and soot volume fraction simultaneously. Note that the emission-derived temperature is dependent on the ratio of the emissivities at the two detection wavelengths, whereas the emission-derived soot volume fraction is dependent on the absolute values of the emissivities. Here, we use $K_a = 6.0$ and $K_e = 8.0$, per our earlier results [1], consistent with Suo-Anttila and Jensen [4].

Source	Symbol	Uncertainty (%) src	$k_{e,\lambda}$	$f_{v,t}$
Diode detector	$I_\lambda/I_{\lambda,0}$	2	4	4
Extinction coefficient	$K_{e,\lambda}$	10	0	10
Path length	s	5	5	5
Test-to-test variability			16	16
		Total:	17	20

Table 1. Transmission measurement uncertainties. The "src" column refers to the uncertainty assigned to the source. The columns for $k_{e,\lambda}$ and $f_{v,t}$ show the source uncertainties multiplied by the sensitivity coefficients. The total uncertainty is the root-mean-square sum of the individual uncertainties.

Source	Symbol	Uncertainty (%) src	$f_{v,e}$	T_e
APD detectors	$\tilde{V}$	4	16	1
Absorption coefficient	K_a	20	20	0
	ΔK_a	3	33	3
Path length	s	5	5	0
Test-to-test variability			42	7
		Total:	60	8

Table 2. Emission measurement uncertainties. The format is the same as Table 1.

Measurement Uncertainty

A full uncertainty analysis was presented for the soot absorption/emission diagnostic in Ref. [1]. The results of that analysis are summarized in Tables 1 and 2. Unlike the previous study, the experiments in this study were repeated two or three times at many of the measurement locations. This repetition allows an assessment of the statistical uncertainty in the measurements caused by test-to-test variability.

Since almost all of the measurement uncertainty (not including test-to-test variability) is due to uncertainties in analysis input parameters, these uncertainties are systematic, rather than random. Thus, these uncertainties are not responsible for any scatter in the values of the measurements; this scatter is attributed entirely to test-to-test variability. The variance in the measurement due to this variability at a particular point in the fire is assumed equal to the calculated variance, σ^2, in that measurement for the repeated tests. The 95% confidence interval for that measurement due to test-to-test variability is then estimated as $t_{n-1,0.95}\,\sigma/n^{1/2}$, where n is the number of tests at that point and $t_{n,\alpha}$ is the value of Student's

t variable such that Probe$[t_n > t_{n,\alpha}] = \alpha/2$. Typical values of this 95% confidence interval for the various measurements are listed in Tables 1 and 2.

Species Measurement

Tunable diode laser absorption spectroscopy (TDLAS) was performed in this series of tests to detect three species: H_2O, C_2H_2, and CH_4. To obtain the required sensitivity, we use a Herriott cell configuration with one-inch mirrors at a set spacing allowing eighteen optical passes across the 36.5 mm × 1.5 cm dia. cylindrical probe volume. The TDLs are multiplexed together and transmitted through a common optical path. The driving signals for the TDLs consist of a high-frequency (~1 MHz) modulation superimposed upon a low-frequency (890 Hz) ramp. The high frequencies are varied for the individual lasers so that they can be de-multiplexed by using separate lock-in amplifiers for each frequency (frequency-division multiplexing). The data acquisition and TDL hardware allow one spectral scan, 98 points in length and nominally 0.15 nm in spectral width, for each channel every 1.12 ms. The phases of the lock-in amplifiers were adjusted while flowing a calibration gas mixture containing acetylene and methane through the end of the probe.

The TDL waveforms were ensemble-averaged to improve signal to noise and were normalized by the average value of the 0f signal [5]. Then the magnitude a of the 2f absorption peak was measured. To determine species partial pressure from line strength, the measurement must be scaled with a reference cell line strength a_{ref} measured at temperature T_{ref} and partial pressure of p_{ref} measured in a cell with a path length of s_{ref}. This is done using the following equation:

$$p_i = \frac{p_{\text{ref}}}{\sigma(T)} \frac{a}{a_{\text{ref}}} \frac{s_{\text{ref}}}{s} \tag{6}$$

Here, $\sigma(T)$ is line strength as a function of temperature normalized by the line strength at the reference temperature, and can be determined from models such as those described by Herzberg [6], from the HITRAN and HITEMP molecular spectroscopy databases [7,8], or from experimental measurements reported in the literature. Changes in gas density with temperature are included in the $\sigma(T)$ line strength function. In the case of water vapor, soot temperature is used for the correction with the assumption that the water vapor is, on average, at the same temperature as the soot. This assumption is a poor one for the fuel species, C_2H_2 and CH_4. Soot and product species such as H_2O tend to be present close to the flame sheet and in hot post flame regions, while fuel species tend to be present in the cooler pre-flame regions. Thus, we assume that C_2H_2 and CH_4 are present only in regions with characteristic temperatures: $T_{C_2H_2} = 1200$ K and $T_{CH_4} = 1000$ K, respectively.

The modulation of the laser couples nonlinearly with the linewidth to change the measured line strength. Transitions that exhibit significant changes in linewidth with temperature are affected the most. The reference cells are maintained at a reduced pressure, 53 kPa (400 torr), to produce lineshapes that are nominally the same width as those produced by species at flame temperatures.

The H_2O absorption measurement was made using an overtone transition at 1309.68 nm

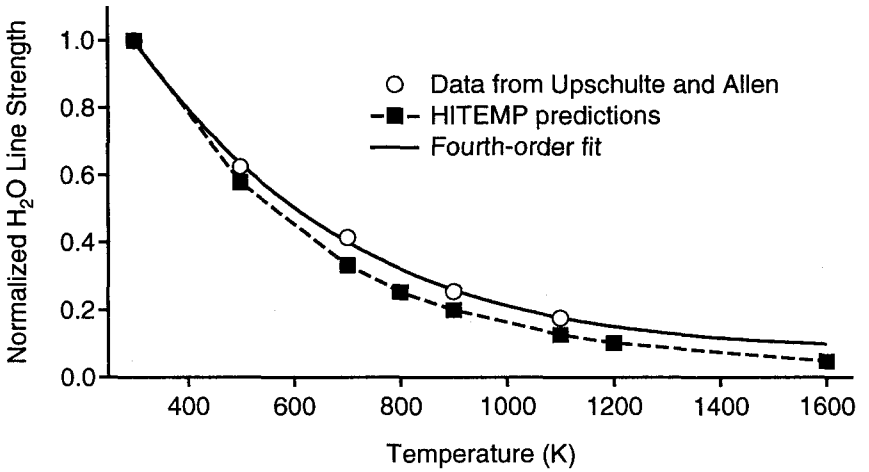

Figure 1. Comparison of measurements of water vapor line strength by Upschulte and Allen to predictions using the HITEMP database. The fourth-order fit is used to correct the measured line strength for the effects of temperature.

(v'–v'' = 000–002, ϕ'–ϕ'' = 4,3,2–5,4,1). This transition was characterized recently by Upschulte and Allen [9]. Their data, consisting of measurements of H_2O line strength as a function of temperature up to 1100 K, show significant differences from predictions using the HITEMP database. When the effect of gas density is included, however, the differences are smaller. A fourth-order polynomial was used to correct our measurements for temperature effects. The polynomial coefficients were calculated directly from Upschulte and Allen's data, with density effects included, using least-squares linear regression. This resulting relation, shown in Fig. 1, is $\sigma_{H_2O}(T) = 1.89 - 3.84\tilde{T} + 3.25\tilde{T}^2 - 1.29\tilde{T}^3 + 0.20\tilde{T}^4$, where $\tilde{T} = T/1000$ K.

The CH_4 absorption measurement was made using transitions in the R(6) manifold of the $2\nu_3$ band. The measured line, characterized by Nagali et al. [10] is a combination of six transitions between 1645.53 nm and 1645.57 nm. Nagali et al. recommend a simple harmonic oscillator-rigid rotator model for determining the variation of line strength with temperature. This calculation is outlined in Appendix A.

The C_2H_2 absorption measurement was made using a $\nu_1 + \nu_3$ transition at 1539.43 nm. This transition is the one assigned $P(23)$ by Kou et al. [11]. The simple harmonic oscillator-rigid rotator model also gives good results for this molecule [12].

Calculated line strength variations with temperature for both molecules are shown in Fig. 2. Since methane and acetylene are assumed to be present at a single characteristic temperature (see above), we set $\sigma_{C_2H_2} = \sigma_{C_2H_2}(T_{C_2H_2}) = 0.0616$ and $\sigma_{CH_4} = \sigma_{CH_4}(T_{CH_4}) = 0.0474$.

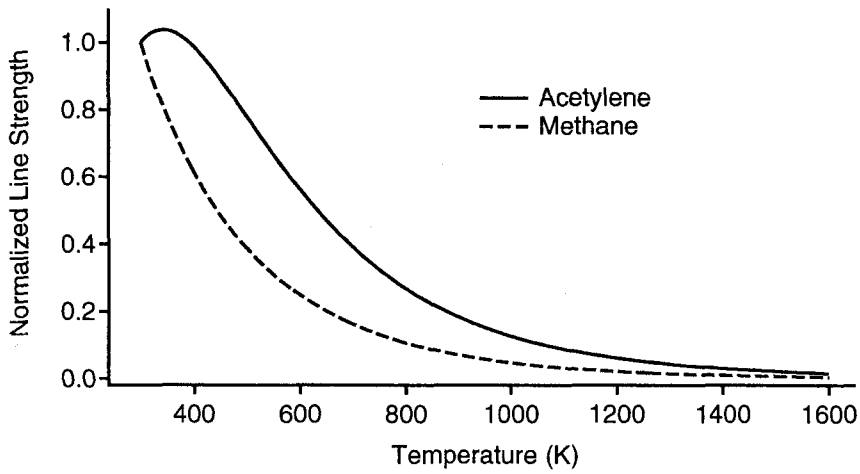

Figure 2. Calcuated line strength variations with temperature of acetylene and methane. The calculations were performed using the simple harmonic oscillator-rigid rotator model outlined in Appendix A.

Summary of Experiments Performed

A series of tests was conducted in July 2003 at Sandia's FLAME (Fire Laboratory for Accreditation of Models and Experiments) facility at the Lurance Canyon Burn Site near Albuquerque, New Mexico. This facility is fully described in Refs. 13 and 14; a brief description is given here.

JP-8 fuel was floated in a 2 m diameter pan on a layer of water nominally 10.0 cm deep. 38 L (10 gal) of JP-8 were used for each test, giving a layer of JP-8 approximately 1.2 cm thick. The water was either replaced or allowed to cool substantially after each test to ensure repeatability from test to test. Air was injected into a honeycomb ring on the floor 1.8 m below the bottom of the pan. The temperature profile of the fuel and water in the pan was monitored with an array of thermocouples during the tests. The temperatures of the ambient air, forced air, and facility walls were monitored with thermocouples as well. The instantaneous fuel depth was monitored with a differential-pressure transducer. The fuel regression rate was calculated by applying a linear regression to the fuel depth data over the time interval of the analysis. The specific gravity of the fuel was assumed to be 0.8 [15]. The differential-pressure gauge did not work correctly for all of the tests. In the cases where gauge data were not available, the burning rate was estimated from the temperature profile in the fuel.

The measurement probe, fully described by Shaddix et al. [16], is a water-jacketed probe formed by two concentric, square aluminum tubes. The overall outer dimension of the tubing is 8.9 cm (3.5 in), while the innermost dimension is 5.7 cm (2.25 in). The probe's two arms hang downward, on either side of the measurement volume, from a straight section cantilevered over the fire. The distance between the outer edges of the two arms is 43 cm

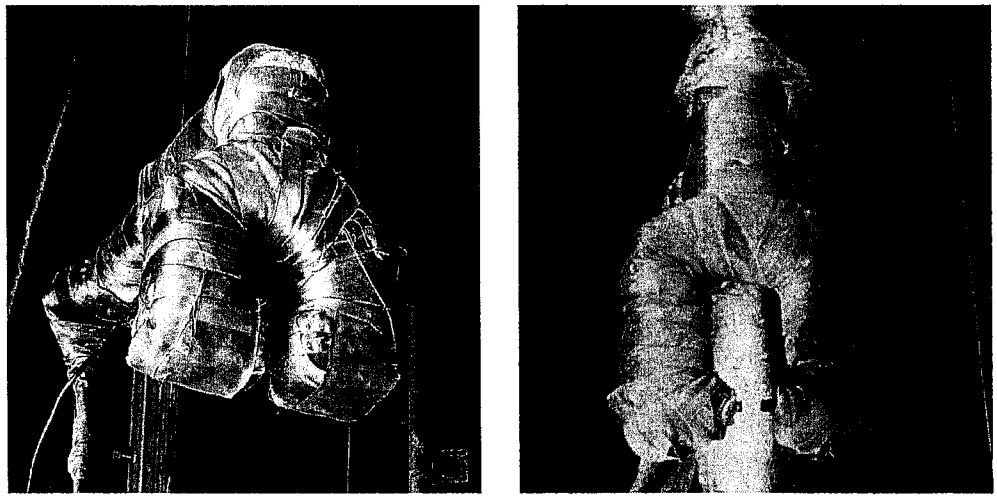

(a) August 2002 (b) July 2003

Figure 3. The probe insulation. Comparison between (a) the previous test series [1] and (b) the current test series.

(17 in) (without the insulation). Two 2.5 cm (1.0 in) diameter steel sight tubes extend from the ends of the probe arms to the edges of the probe volume. These sight tubes do not have water jackets; their smaller bulk compared to the rest of the probe minimizes disruptions to the flowfield in the vicinity of the probe volume. The vertical drop from the top of the supporting beam to the bottom surfaces of the two arms is 76 cm (30 in).

Previous experience [1] with this probe indicated that insulation approximately 5 cm thick is required on all surfaces to keep it cool during the fire. The resulting cross-sectional outer dimension of the arms forming the probe head was 18.9 × 18.9 cm. An effort was made, however, to reduce the amount of insulation in the vicinity of the measurement volume. Pictures of the probe insulation from this test series and the previous series are shown in Fig. 3.

A helium purge was used to keep the internal optics of the probe free of soot. Helium was chosen as the purge gas because of its relatively small refractive index. The helium was forced through the interior of the probe and exited from the two optical ports into the probe volume.

Measurements were made in a total of thirty-five two-meter diameter pool fires, each providing approximately four minutes of quasi-steady burning. The probe position was fixed for the duration of each test. Measurements were performed on the centerline from 0.5 m to 2.0 m above the fuel surface, at increments of 0.25 m, to characterize the axial profile of the fire. The radial profile was characterized with measurements from 0.0 m to 0.6 m from the centerline at a height of 1.0 m above the fuel surface. Tests at some of the probe positions were performed three or four times to gauge the repeatability of the measurements. Tests were also performed with the flow of air through the honeycomb ring

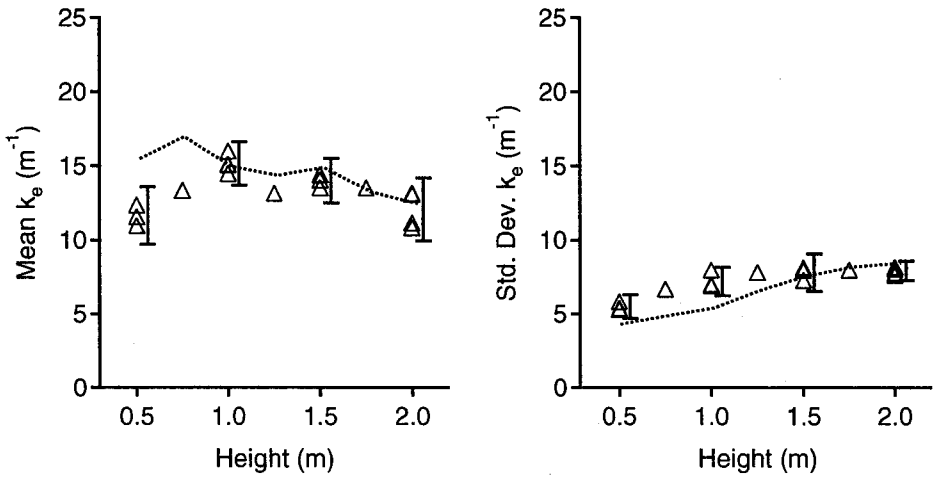

Figure 4. Extinction coefficient on the centerline as a function of height. The symbols represent individual fires. The error bars, which are offset from the data, show the range of the estimated 95% confidence intervals for the data. The dotted line shows results from Ref. 1, where the probe was positioned 0.1 m from the centerline.

changed to twice of the baseline value and one-half of the baseline value to investigate the effect of the air flow. Finally, one test was performed with a reduced probe-volume length to determine the effects of spatial averaging on the results. Table 3 summarizes the operating conditions for the thirty-five tests.

Results

Soot Measurements

Figure 4 shows averages and standard deviations of the soot extinction coefficient from measurements made on the centerline of the fire. The standard deviations are indicative of the breadth of measured probability density function (PDF). Error bars are also shown on the graphs to indicate the 95% confidence region for the data, calculated from the estimates of uncertainty and the experimental scatter observed among tests in the same location. The data compare very favorably with data taken in nominally identical fires in the previous study [1]. In the previous study, the probe support did not allow it to reach the centerline, so measurements were taken 0.1 m from the centerline.

Figures 5 and 6 show the measured axial profiles of soot concentration and temperature, respectively. Again, the results compare favorably with Ref. 1. Temperature is lower than previously measured by 50–100 K. Measurements of the radial temperature profile, presented below, indicate that the temperature is expected to be 50–100 K higher at a radial position of 0.1 m than on the centerline, so these results are consistent. At a height of

Test	Probe position[a] Height (m)	Radius (m)	Analysis Start[b] (s)	Length (s)	Fuel Regression (mm/min)	Initial Temp. Water (°C)	Fuel (°C)	Wall Temp (°C)	Ambient Temp[c] (°C)	Blowers Flow (m^3/min)[d]	Temp (°C)
1	1.00	0.0	59	176	1.8[e]	36.7	40.8	35.1	42.5	460	39.4
2	1.00	0.0	49	176	1.6	40.6	44.6	39.4	41.4	460	39.0
3	1.00	0.0	79	176	1.3	42.0	45.5	42.8	41.1	457	39.0
4	1.00	0.0	40	192	1.4	36.1	37.8	33.2	40.0	443	37.6
5	1.00	0.2	38	176	1.6	41.0	42.6	37.2	40.2	460	37.8
6	1.00	0.3	47	192	1.8	42.4	44.8	40.5	40.6	460	37.9
7	1.00	0.3	43	176	1.8	42.7	44.1	43.6	41.5	457	38.3
8	1.00	0.3	34	192	1.9	34.6	35.1	31.7	36.4	460	33.2
9	1.00	0.6	46	192	2.1	36.8	38.8	34.3	36.6	460	34.0
10	1.00	0.5	41	192	2.0	38.8	40.4	37.3	37.8	460	35.2
11	1.00	0.6	32	192	2.0	38.8	42.2	40.2	38.3	460	36.0
12	1.00	0.4	34	192	2.0	38.9	42.8	42.5	39.8	460	38.1
13	1.00	0.6	45	192	2.0	42.0	46.8	45.5	40.7	460	38.6
14	1.00	0.1	53	176	2.0	42.8	47.3	48.5	42.0	460	39.3
15	2.00	0.0	35	192	2.0	35.8	33.4	33.1	36.7	460	30.9
16	2.00	0.0	34	208	2.0	39.7	37.4	35.2	38.3	460	32.1
17	1.50	0.0	39	192	2.0	40.4	40.7	37.0	42.0	460	38.2
18[f]	1.50	0.0	56	192	1.6[e]	31.9	32.3	28.9	37.0	460	30.6
19	1.50	0.0	38	208	1.8[e]	35.9	37.8	32.0	38.4	460	32.4
20	1.50	0.0	38	208	2.1	37.9	40.1	35.1	40.1	460	32.4
21	0.50	0.0	40	192	2.0	38.3	37.7	37.9	40.2	460	33.9
22	0.50	0.0	36	192	2.3[e]	40.3	42.9	41.1	39.9	460	34.4
23	0.50	0.0	40	208	2.0	40.6	40.6	43.4	40.3	460	34.0
24	0.75	0.0	31	208	2.1	40.8	41.5	46.0	39.9	460	34.8
25	1.25	0.0	26	208	2.2	41.0	42.6	48.3	39.8	460	34.9
26	1.75	0.0	30	208	2.0	42.1	43.2	50.1	39.5	460	34.9
27	2.00	0.0	40	208	1.9[e]	36.8	32.8	33.5	32.5	460	27.3
28	2.00	0.0	38	208	2.1	37.6	36.7	35.4	32.0	460	26.9
29	1.00	0.0	40	208	2.0[e]	40.8	37.8	34.7	36.3	231	34.1
30	1.00	0.0	30	208	2.4[e]	38.9	39.7	38.2	36.3	921	30.4
31	1.00	0.0	35	208	1.5[e]	38.2	34.6	39.7	34.9	230	27.7
32	1.00	0.0	32	192	1.8[e]	31.0	31.1	28.0	33.1	918	29.3
33	1.00	0.0	41	208	2.2	34.5	36.5	30.4	34.0	230	29.9
34	1.00	0.0	26	208	1.5[e]	35.3	36.4	33.7	36.0	920	31.4
35	1.00	0.0	35	208	2.0[e]	33.7	35.4	35.7	37.8	460	32.0
				Average:	1.9	38.5	39.6	38.0	38.4		34.2
				Std. Deviation:	0.2	3.1	4.2	5.6	2.8		3.7

[a] Uncertainty ±1 cm. [b] Time from ignition. [c] Inside enclosure, before ignition. [d] Standard conditions (300 K, 101 kPa). [e] Estimated from thermocouple rake data. [f] This test was not included in the analysis due to problems with the emission signals.

Table 3. Operating conditions for the tests.

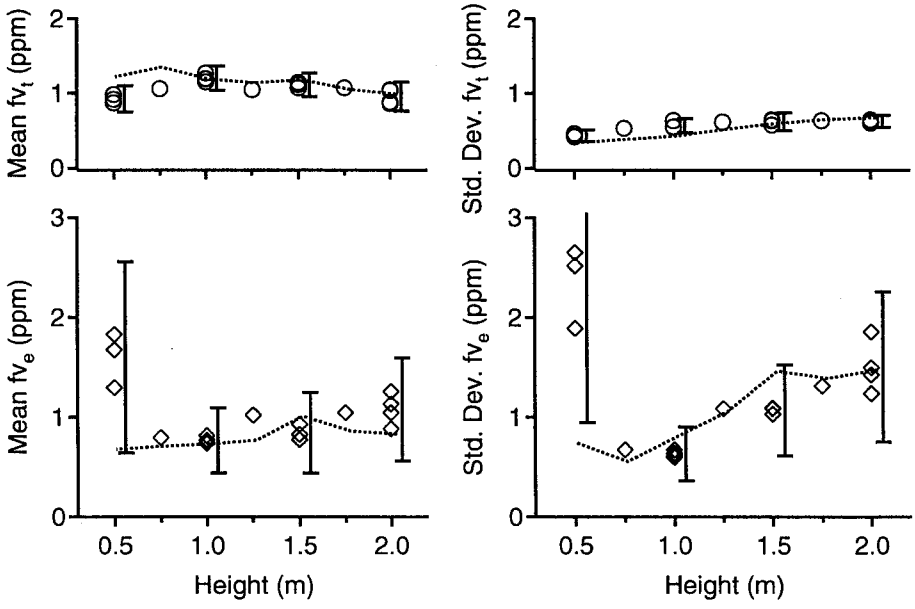

Figure 5. Soot concentration on the centerline as a function of height. Symbols, error bars, and lines are as described in Fig. 4.

0.5 m, the mean value of emission-based soot volume fraction is significantly larger than the corresponding transmission-based value. The error bars in Fig. 5, however, indicate that the difference is not significant, given the uncertainties in the measurement. The 0.5 m high centerline measurement location is probably in the vapor-dome region of the fire. Thus, the uncertainties in optical constants are especially severe [17] due to the likely presence of tar aerosols.

Figures 7–9 show the radial profile of the measured soot properties 1.0 m above the fuel surface. Moving out from the centerline, temperature increases and soot concentration decreases until we pass 0.3 m. At 0.4 m from the centerline, mean temperature falls. Both temperature and emission-based soot concentration become much more variable at these distances. This is because we are outside of the mean flame envelope and the flame is only intermittently entering the probe volume. Much of the soot passing through the probe volume at these positions is smoke from previously-quenched flames that is in the process of cooling through net radiation loss and mixing with air.

Figures 10–12 show variations in the measurements in the middle of the fire with facility air flow rate. At high air flow rates there are lower soot concentrations and somewhat higher temperatures. This trend is consistent with more intense mixing of the air with the fire plume.

Table 4 summarizes the results for the mean values and standard deviations of the soot extinction coefficient, soot volume fraction, and soot temperature. Both the radial and axial profiles are presented, as well as variation with facility air flow. The uncertainties in the

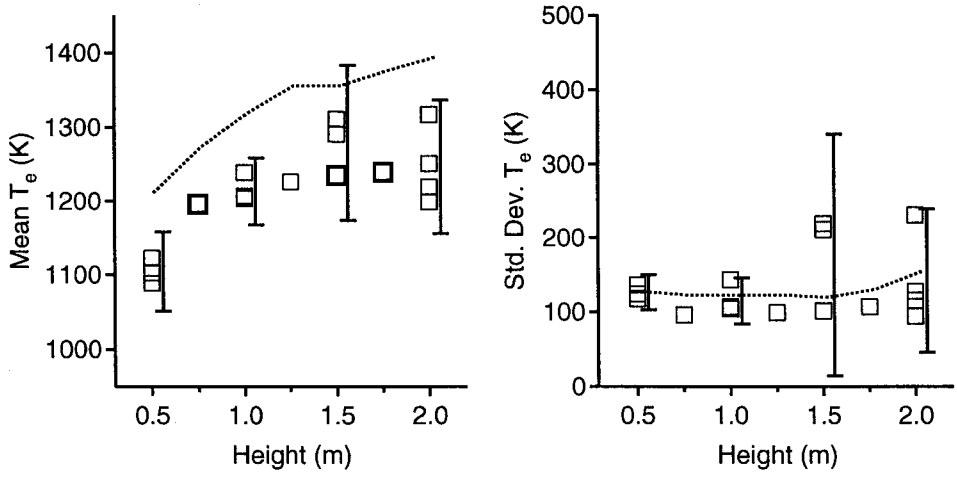

Figure 6. Soot temperature on the centerline as a function of height. Symbols, error bars, and lines are as described in Fig. 4.

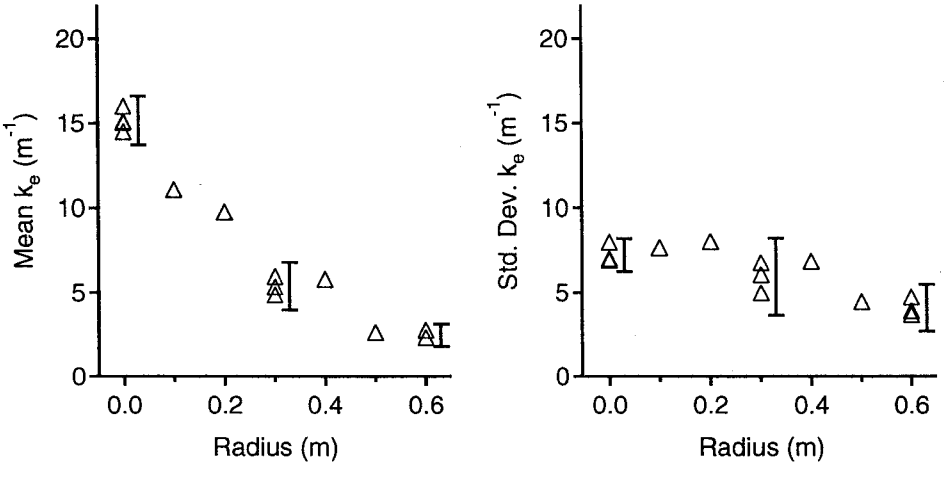

Figure 7. Extinction coefficient at 1.0 m high in the fire as a function of radius. Symbols, error bars, and lines are as described in Fig. 4.

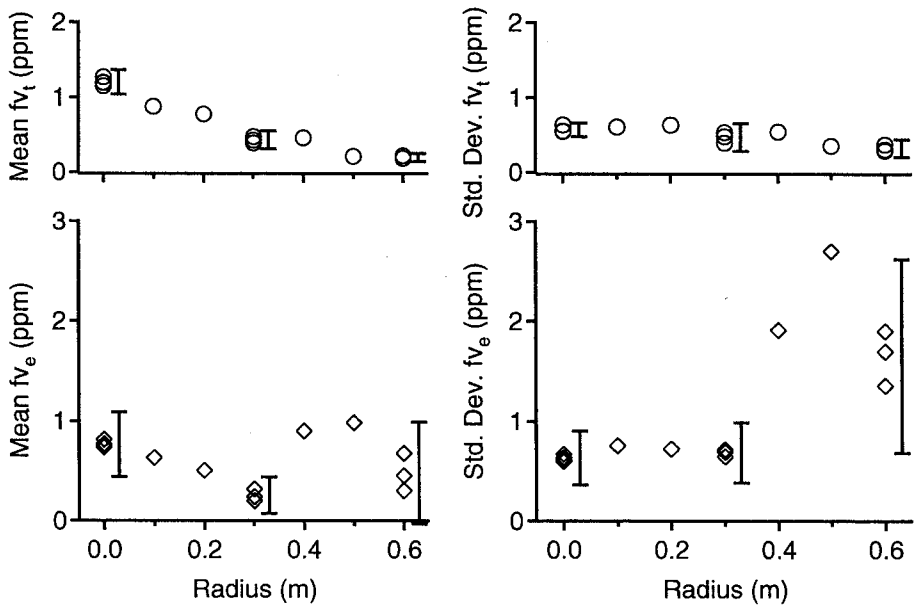

Figure 8. Soot concentration at 1.0 m high in the fire as a function of radius. Symbols, error bars, and lines are as described in Fig. 4.

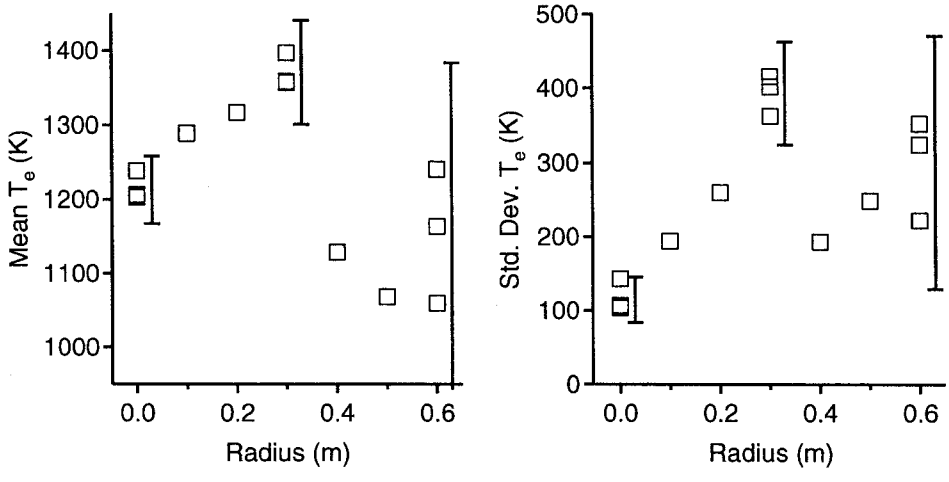

Figure 9. Soot temperature at 1.0 m high in the fire as a function of radius. Symbols, error bars, and lines are as described in Fig. 4.

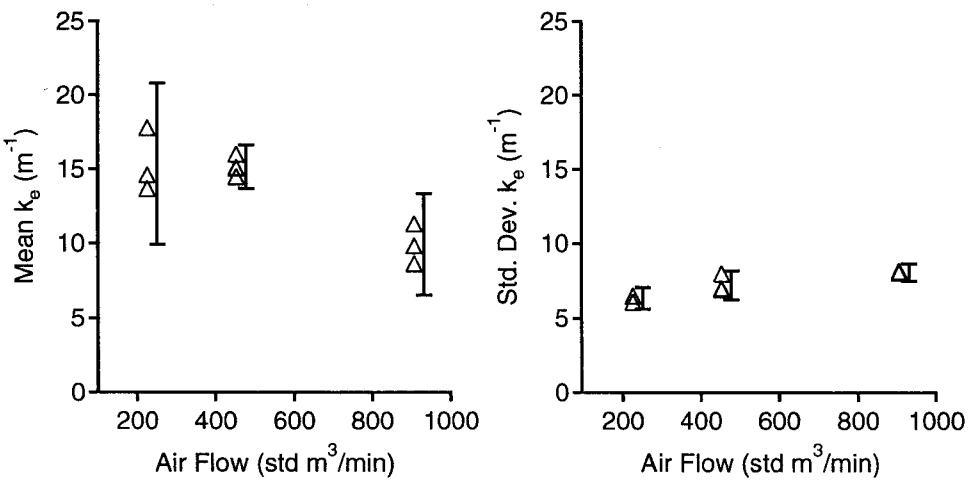

Figure 10. Soot extinction as a function of air flow, at the centerline 1.0 m above the fuel surface. Symbols, error bars, and lines are as described in Fig. 4.

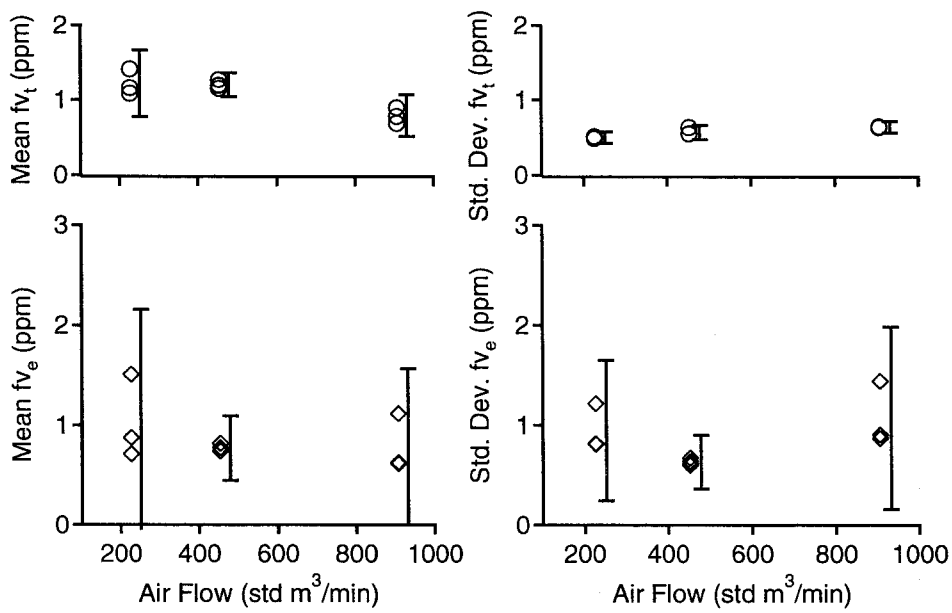

Figure 11. Soot concentration as a function of air flow at the centerline 1.0 m above the fuel surface. Symbols, error bars, and lines are as described in Fig. 4.

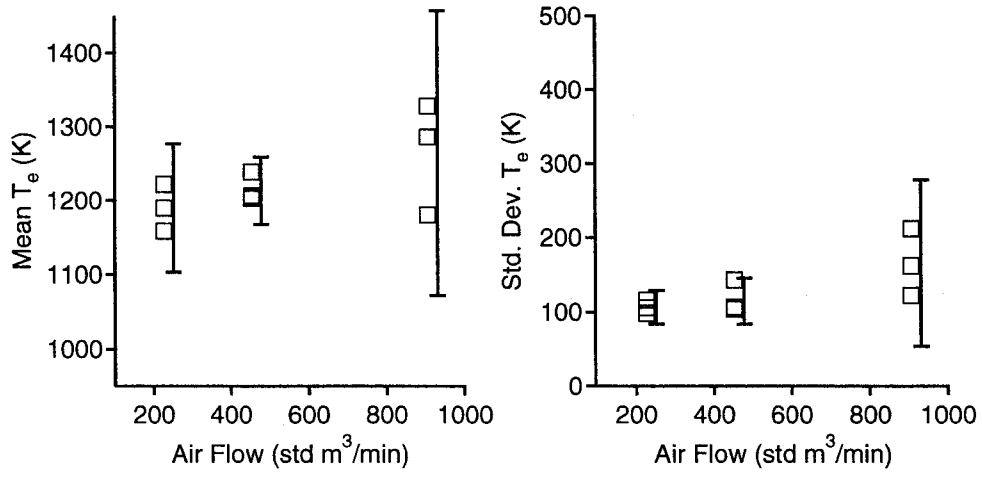

Figure 12. Soot temperature as a function of air flow at the centerline 1.0 m above the fuel surface. Symbols, error bars, and lines are as described in Fig. 4.

measurements are the estimated 95% confidence intervals calculated from the combination of test-to-test variability and uncertainties in the analysis parameters.

Probability Density Functions

Figure 13 shows probability density functions (PDFs) of soot concentration and soot temperature on the centerline as a function of height. The double-peaked structure that evolves with height is discussed in more detail in Ref. [1]. Only the measurement locations where multiple tests were performed are shown. The figures show that the structure of the PDF is repeatable.

Figure 14 shows PDFs of soot volume fraction and temperature measured at a height of 1.0 m as a function of radius. We see that the double-peaked structure of the PDFs goes away as we move outward from the centerline and soot is favored in low concentrations. The distributions measured 0.3 m from the centerline show low soot volume fractions and high temperatures, perhaps indicative of soot present in active oxidation zones. At a radius of 0.6 m, low soot concentrations are present over a wide distribution of temperatures, supporting the interpretation that cooling smoke is present at this position.

Figure 15 shows the variation in the middle of the fire of the soot volume fraction PDF and soot temperature PDF as a function of air flow. At high air flow (960 std m^3/min), the PDF shifts from predominantly high soot volume fraction to predominantly low soot volume fraction. This is evidence of the reduction in fire height that is observed visually at high air flows. The reduced fire height is a result of the more intese fuel-air mixing present with the higher air flow.

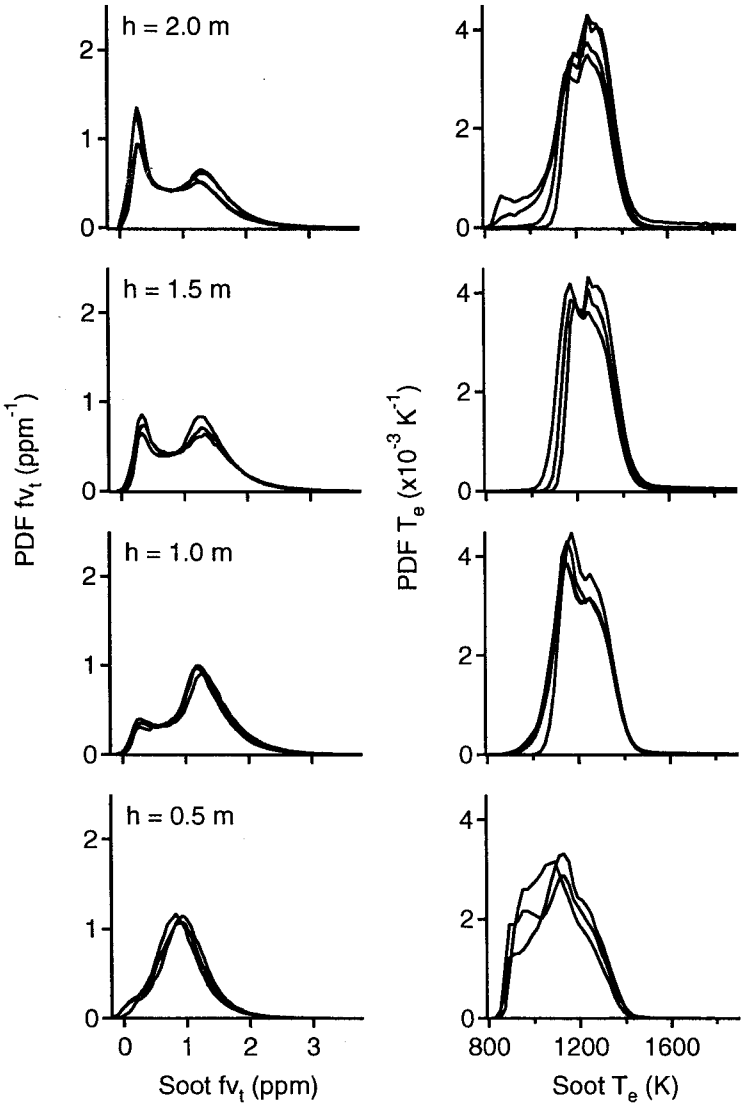

Figure 13. PDFs of soot concentration and temperature as a function of height along the centerline. The lines show results from multiple tests with the probe in the same position.

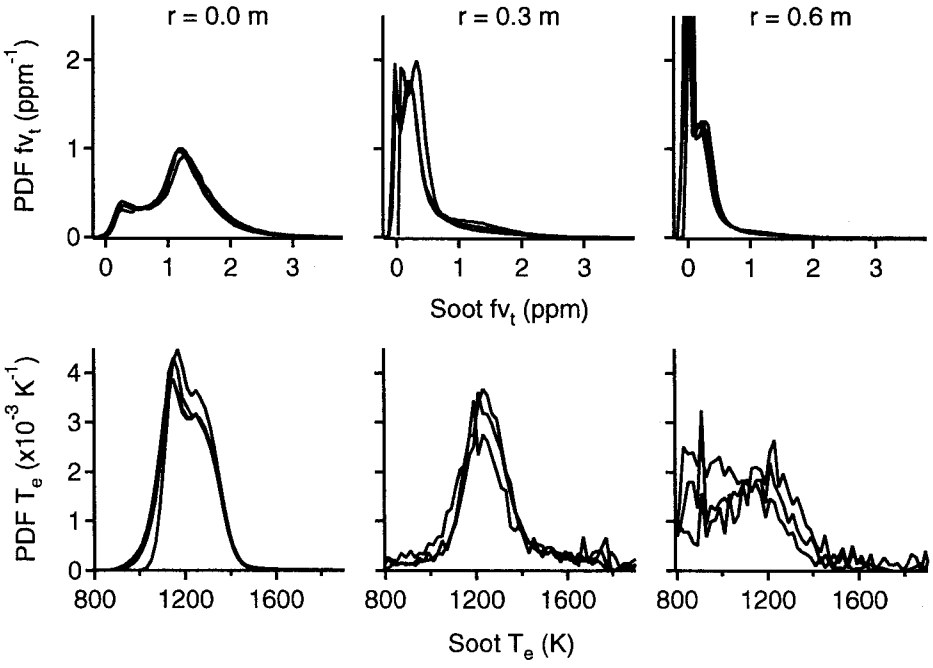

Figure 14. PDFs of soot concentration and temperature as a function of radius at a height of 1.0 m.

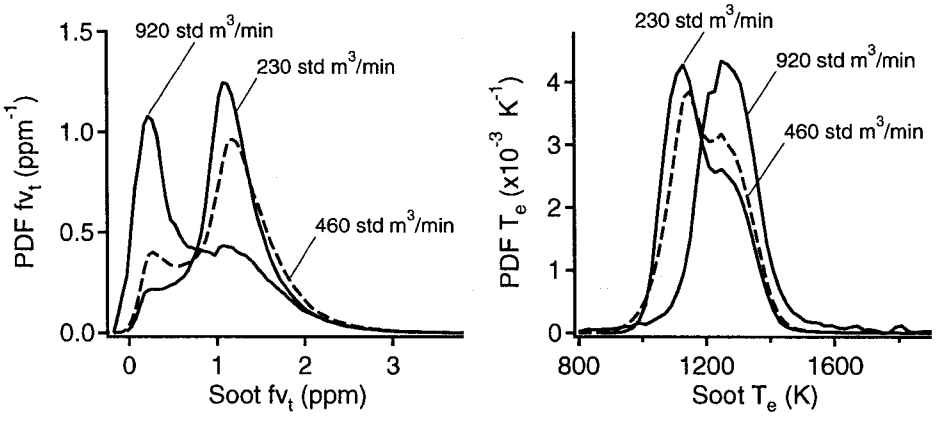

Figure 15. PDFs of soot concentration and temperature as a function of air flow, at a height of 1.0 m along the centerline.

Height[a] (m)	Radius[a] (m)	Air Flow (m^3/min)[c]	Soot Extinction Mean (m^{-1})	Soot Extinction StDev (m^{-1})	Soot volume fraction[b] Mean (ppm)	Soot volume fraction[b] StDev (ppm)	Soot Temperature Mean (K)	Soot Temperature StDev (K)
Axial profile:								
0.5	0.0	460	11.6 ±1.9	5.5 ±0.8	0.92 ±0.18	0.44 ±0.08	1105 ± 54	126 ± 23
1.0	0.0	460	15.2 ±1.5	7.2 ±1.0	1.20 ±0.16	0.57 ±0.10	1213 ± 45	115 ± 31
1.5	0.0	460	14.0 ±1.5	7.8 ±1.3	1.11 ±0.16	0.62 ±0.12	1279 ±105	177 ±163
2.0	0.0	460	12.1 ±2.1	7.9 ±0.7	0.96 ±0.19	0.63 ±0.08	1246 ± 90	142 ± 97
Radial profile:								
1.0	0.0	460	15.2 ±1.5	7.2 ±1.0	1.20 ±0.16	0.57 ±0.10	1213 ± 45	115 ± 31
1.0	0.3	460	5.4 ±1.4	5.9 ±2.3	0.43 ±0.12	0.47 ±0.19	1371 ± 70	394 ± 69
1.0	0.6	460	2.5 ±0.7	4.1 ±1.4	0.20 ±0.06	0.33 ±0.12	1155 ±229	300 ±171
Air flow variation:								
1.0	0.0	230	15.4 ±5.4	6.3 ±0.7	1.22 ±0.45	0.50 ±0.08	1190 ± 87	107 ± 23
1.0	0.0	460	15.2 ±1.5	7.2 ±1.0	1.20 ±0.16	0.57 ±0.10	1213 ± 45	115 ± 31
1.0	0.0	920	9.9 ±3.4	8.1 ±0.6	0.79 ±0.28	0.64 ±0.08	1265 ±192	166 ±112

[a] Uncertainty ±1 cm. [b] Extinction-based measurement. [c] Standard conditions (300 K, 101 kPa).

Table 4. Summary of experimental results.

Spectral Density Functions

Power spectral densities (PSDs) were used to examine the frequency content of the signals. Fast Fourier transforms were applied to sixteen-second blocks of data. All of the FFTs from a single experiment were then averaged together to estimate the PSD.

The PSDs for the transmission-based soot volume fraction data are shown in Fig. 16 for heights of 1.0 m and 2.0 m on the centerline. The peaks in the PSDs at the puffing frequency (0.94 Hz in these fires) are clearly visible. A second harmonic of the puffing frequency is also visible. At 2.0 m high in the fire, the second harmonic is stronger. Otherwise, the PSDs are very similar, except for a slightly weaker spectrum in the frequency range of 20–400 Hz for the 2.0 m data.

There is also a very sharp break in the slope of the PSD around 12 Hz. (The break is more visible in Figs. 18 and 20.) The PSD then flattens some before beginning to fall off again. The average slope over the higher frequency ranges (100–1000 Hz) is close to that predicted by the Kolmogorov spectrum law for isotropic, homogeneous turbulence (–5/3) [18].

Figure 17 shows a comparison of the soot volume fraction spectra at heights of 0.5 m and 1.0 m on the centerline of the fire. Here, we see that the 0.5 m high PSD is weaker by a factor of approximately 2.5 through the entire frequency range of the spectrum.

Figure 18 shows a comparison of the 1.0 m high, centerline spectrum with one taken 0.6 m from the centerline at the same height. At low frequencies (<2 Hz), the PSDs are

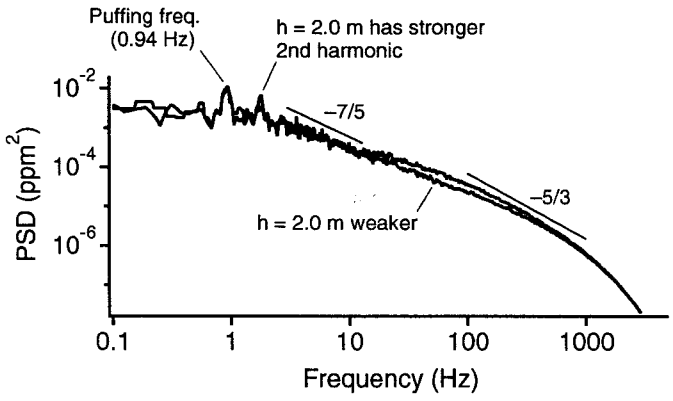

Figure 16. Soot concentration PSD comparison between 1.0 m and 2.0 m high on centerline.

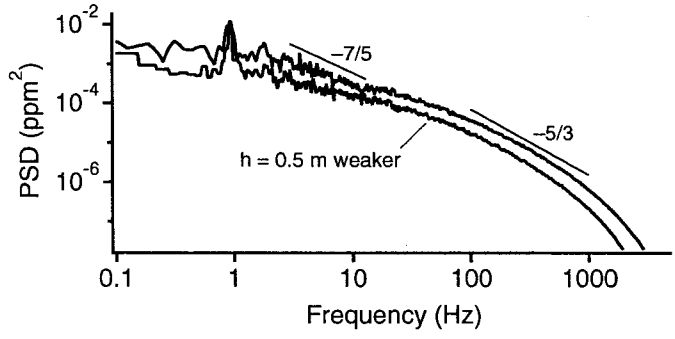

Figure 17. Soot concentration PSD comparison between 1.0 m and 0.5 m high on centerline.

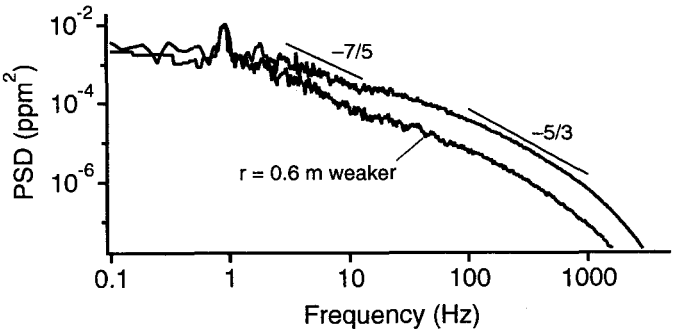

Figure 18. Soot concentration PSD comparison between 0.0 m and 0.6 m radius, 1.0 m high.

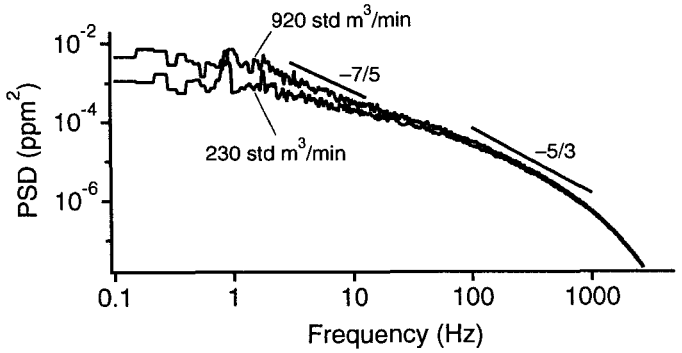

Figure 19. Soot concentration PSD comparison of different air flow rates at 1.0 m high along the centerline.

similar. In the range of 2–12 Hz, however, the PSD at 0.6 m radius falls off more rapidly. Above 12 Hz, the slopes of the two spectra are again similar.

Figure 19 shows power spectra taken at 1.0 m high on the centerline with different rates of facility air flow. The larger air flow increases the energy present at the lower frequencies, i.e. introduces more large-scale turbulence.

Figure 20 shows a comparison of the PSDs for soot concentration and soot temperature at 1.0 m high on the centerline. The behavior of the temperature spectrum is different from soot concentration. For soot temperature, there is no sharp break in slope around 12 Hz. Rather, the spectrum has a slope of about –1 up to about 100 Hz. In the range of 100–1000 Hz, the slope is close to –7/5. Above 1000 Hz, the temperature PSD flattens out; presumably this is a noise floor.

For test number 35, the length of the cylindrical probe volume was reduced by half (18 mm vs. 36 mm). Figure 21 shows a comparison of the spectra from tests with the different lengths. The PSDs are very similar, although the shorter probe volume has slightly less

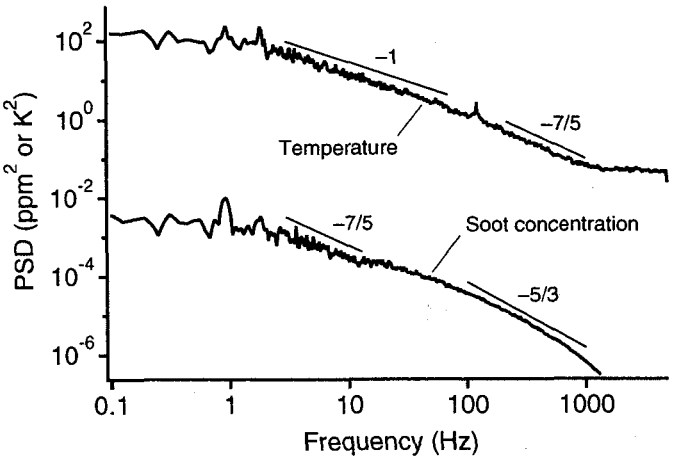

Figure 20. PSD comparison of soot concentration and temperature.

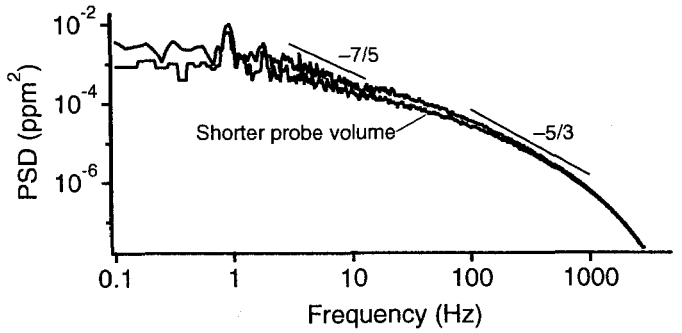

Figure 21. Soot concentration PSD comparison for different probe volume lengths.

energy at frequencies below 100 Hz. This is because the larger flow structures responsible for these lower frequencies are not sampled as effectively with the shorter probe volume.

The frequency exponent for the soot volume fraction data was estimated by fitting a line to the log of spectral power versus the log of frequency for different ranges of frequency. The results are shown in Fig. 22. There are distinct trends in the data with position. At low frequencies (3–10 Hz), on the centerline, low in the fire, the slope is approximately –0.6. As one moves higher in the fire, the slope increases to around –1.1. At higher frequencies (100–1000 Hz), the slope low in the fire on the centerline is very steep (–2.0), but becomes more shallow higher in the fire. The average slope in this frequency range asymptotes to the –5/3 (–1.67) predicted by Kolmogorov spectrum law.

As a function of radius, the PSD slope is relatively constant except at low frequencies. In the frequency range of 3–10 Hz, the slope 1.0 m above the fuel surface and near the center of

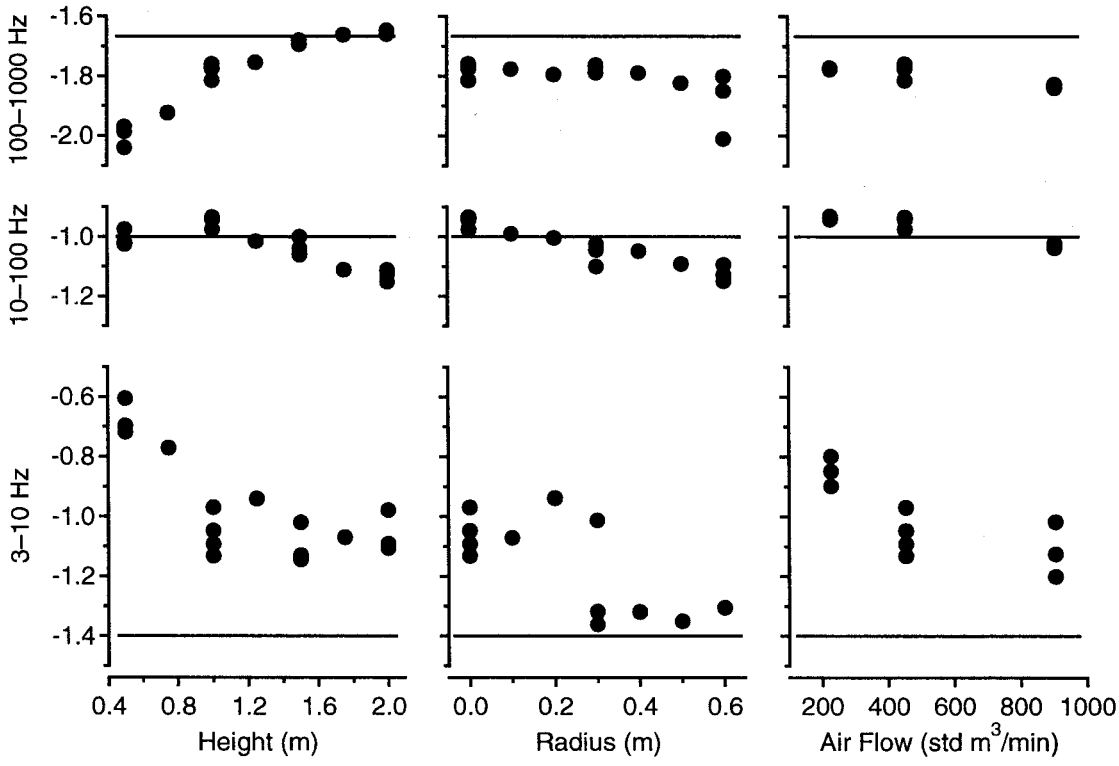

Figure 22. Comparison of soot concentration PSD slope.

the fire is approximately –1.0. At a radius or 0.3 m, however, the slope approaches a value of –7/5 (–1.4), which was predicted by Obukhov [19] and Bolgiano [20] for buoyancy-dominated turbulent flows.

The PSD slope showed little change as a function of air flow. Between the frequencies of 3 Hz and 10 Hz, the slope became larger as air flow was increased.

The spectral power at the puffing frequency was examined as a function of position. The results are shown in Fig. 23. On the centerline, spectral power peaks at approximately 1.5 m in height. As a function of radius at 1.0 m high in the fire, the effect of puffing is weakest on the centerline and at the outer edge (0.6 m radius) of the fire. The effect of puffing is the strongest between 0.2 m and 0.3 m from the center of the fire. This area is where the temperature peaked as well (see Fig. 9), and where the strongest vortical roll-up is expected to occur.

Cross-Correlations

Cross-correlation coefficients were calculated among the various measured quantities by taking the covariance and dividing by the product of the standard deviations. These coef-

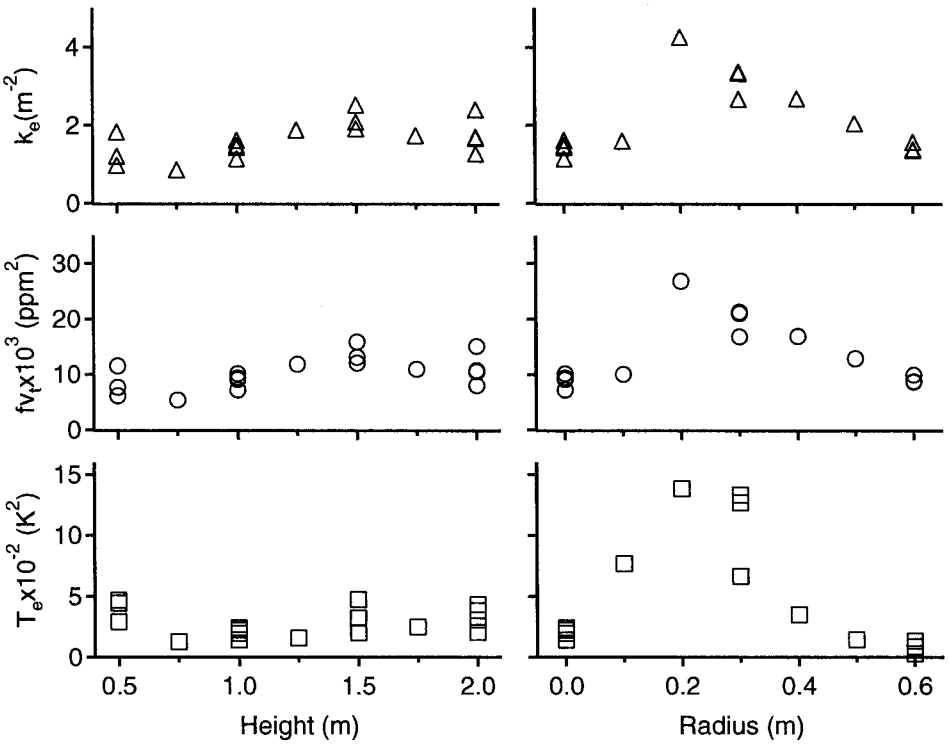

Figure 23. Spectral power at the puffing frequency. Shown as a function of height on the centerline and as a function of radius at 1.0 m high in the fire.

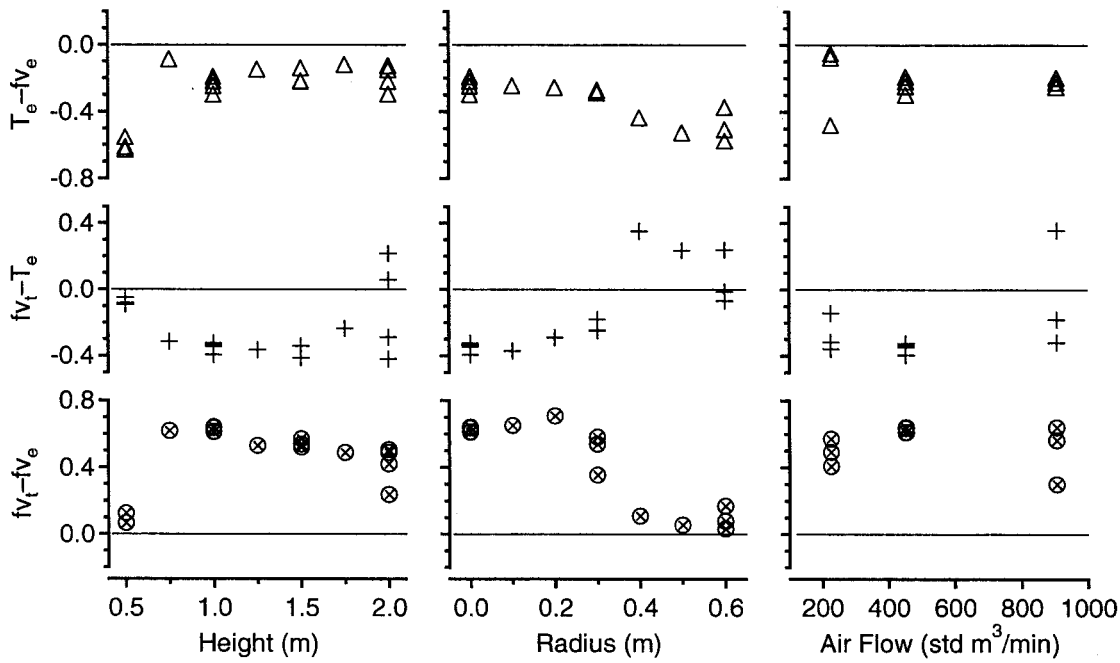

Figure 24. Correlation coefficients.

ficients are shown in Fig. 24. On the centerline, the soot volume fractions from the transmission and emission measurements show a correlation coefficient of approximately 0.5, except at the lowest measurement height. Both soot volume fraction measurements are inversely correlated with soot temperature. This inverse correlation indicates that the larger soot volume fractions correspond to lower temperatures and vice versa.

The correlation coefficients as a function of radial position at 1.0 m high in the fire show a sharp break at 0.3 m from the centerline. Here, the two soot volume fraction measurements become uncorrelated, and the transmission-based soot volume fraction becomes positively correlated with soot temperature. The cross-correlation coefficients show no noticeable trend with facility air flow.

Cross-spectral densities were also computed to examine correlations between soot volume fraction and temperature as a function of frequency. In particular, the phase relations among the quantities were investigated by plotting magnitude and phase of the cross-spectral density as a function of position at the puffing frequency of 0.94 Hz.

The results are shown in Fig. 25. The phase relations are especially interesting. Soot volume fraction and soot temperature are approximately 135 degrees out of phase at most locations in the fire, although they are closer in phase low in the fire and at large radial positions.

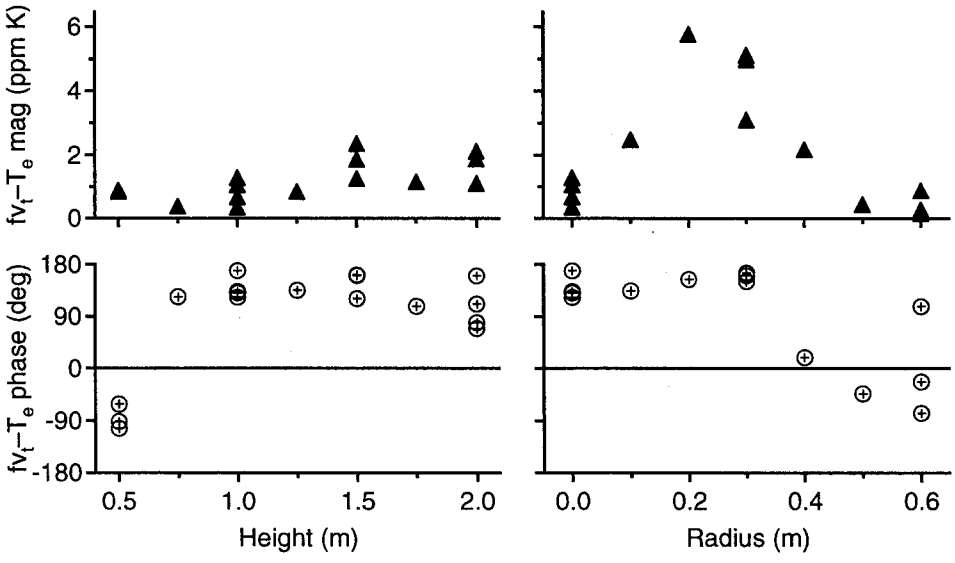

Figure 25. Cross spectral density at the puffing frequency by height.

Species Measurements

Due to the low signal-to-noise of the TDL measurement, the TDL waveforms had to be ensemble-averaged in one-half second sections before the positions of the peaks could be detected. Figure 26 shows a set of TDL waveforms ensemble-averaged over the length of one of the fires.

After ensemble averaging, the effective data rate of the TDL signals was 2 Hz. Also, since the TDL signal is proportional to the TDL 0f signal, the waveforms must be normalized by the TDL 0f signal to get actual line strength. For the data presented here, the TDL waveforms were ensemble-averaged before they were normalized. This procedure improved the signal-to-noise ratio, but effectively weighted the averages by the mean transmitted power of the TDL lasers. Since transmitted power is, in part, related to soot extinction, this weighting produces a bias in the statistics towards situations where there is less soot in the probe volume and therefore more transmitted power.

Figure 27 shows species concentrations on the centerline of the fire. Water vapor concentration appears to peak around 1.5 m above the fuel surface. This is the same location as the peak in the puffing amplitude as determined from the soot volume fraction PSDs (see Fig. 23). Presumably, this location corresponds to the mean height of the active flame zone. Methane and acetylene were detected at locations low in the fire—at 0.5 m and possibly at 0.75 m above the fuel surface—where one would expect them to be primarily located.

Methane and acetylene were not detected in any of the radial positions. Water vapor was detected as these locations, but the intermittent presence of air, which causes only minor

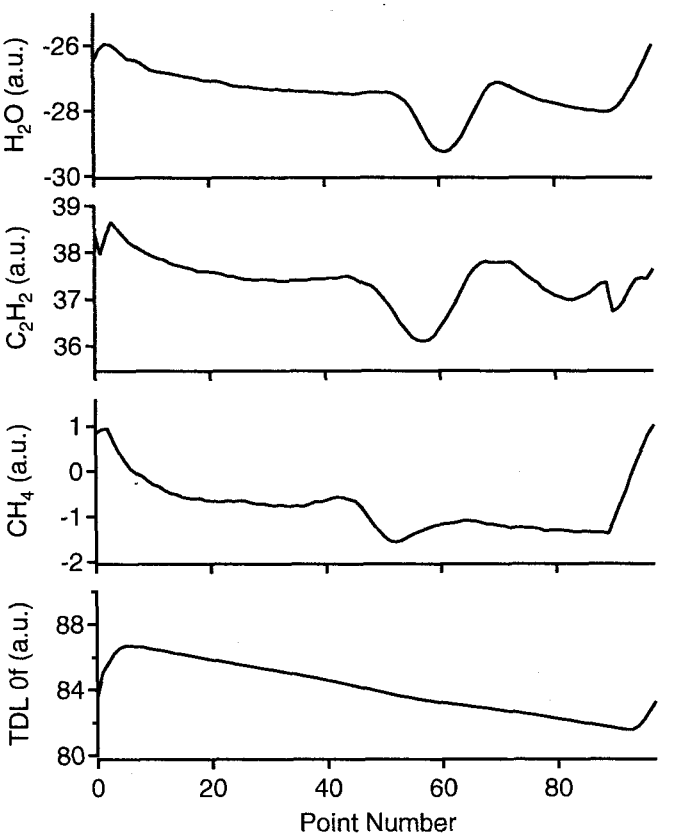

Figure 26. Ensemble-averaged TDL signals.

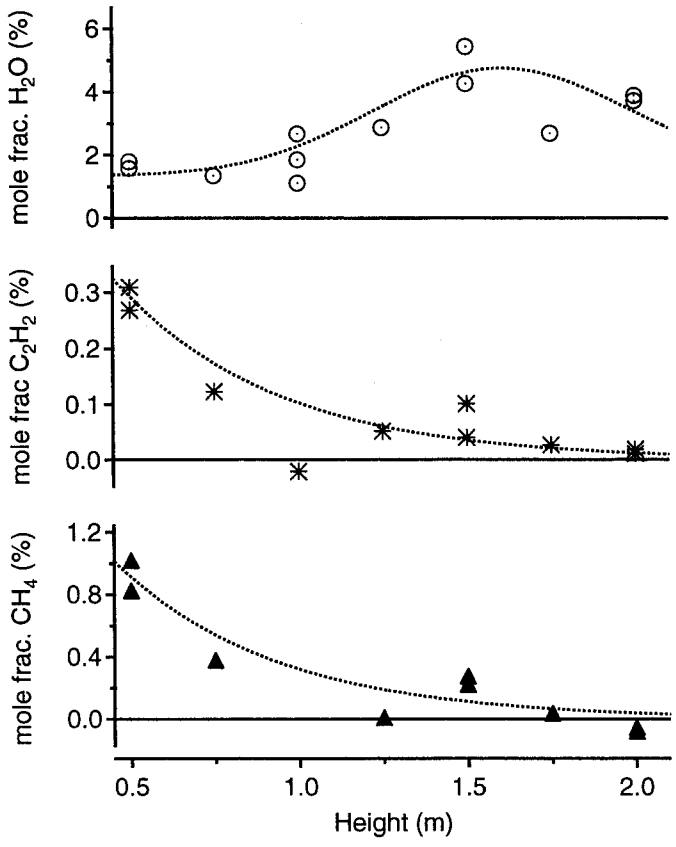

Figure 27. TDL species measurements on the centerline. The dotted lines are curve fits that are included to emphasis the trends in the data.

signal attenuation compared to soot, resulted in the saturation of the data acquisition system. This saturation caused the amount of water vapor present in the air to be overestimated, making measurements at these radial locations unreliable. Therefore, these data are not presented here.

The methane and acetylene concentrations shown in Fig. 27 are meant to be absolute measurements. The water vapor concentration, however, is only proportional to absolute water vapor concentration, because we did not know the absolute concentration of the water vapor present in our reference cell. The value of reference cell concentration we used in the calculations was calculated assuming that saturated water vapor was present in the cell. At this point, the uncertainties present in the TDLAS measurement have not been fully characterized. Therefore, uncertainties for the reported species concentration measurements are not reported here.

Conclusions

Temporally and spatial resolved in situ measurements of transmission- and emission-based soot volume fraction and temperature in a two-meter diameter JP-8 pool fire are reported. Both the axial profile on the centerline of the fire and a radial profile at 1.0 m above the fuel surface are presented. The measurements showed good agreement with a previous study. Multiple tests at the same nominal conditions provided an assessment of test-to-test variability. The effect of the facility air flow rate on the measured soot properties was also studied.

Water vapor, methane, and acetylene concentrations were measured on the centerline of the fire. Water vapor concentration showed a peak at approximately 1.5 m above the fuel surface. Methane and acetylene were detected only at the measurement locations below 1.0 m above the surface.

References

[1] J. J. Murphy and C. R. Shaddix, "Soot Properties and Species Measurements in a Two-Meter Diameter JP-8 Pool Fire," Sandia National Laboratories Report No. SAND2002–8246, June 2003.

[2] M. Q. Brewster, *Thermal Radiative Transfer and Properties*, John Wiley & Sons, Inc., New York, NY, 1992.

[3] J. J. Murphy and C. R. Shaddix, "Influence of Scattering and Probe-Volume Heterogeneity on Soot Measurements using Optical Pyrometry," *Combustion and Flame*, (2003). submitted Dec. 2003.

[4] J. M. Suo-Anttila and K. A. Jensen, private communication, 2003.

[5] J. Henningsen and H. Simonsen, "Quantitative Wavelength-Modulation Spectroscopy Without Certified Gas Mixtures," *Applied Physics B*, 70(4):627–633 (2000).

[6] G. Herzberg, *Molecular Spectra and Molecular Structure. Volume II: Infrared and Raman Spectra of Polyatomic Molecules*, Krieger Publishing Co., Malabar, FL, 1991.

[7] L. S. Rothman, C. P. Rinsland, A. Goldman, S. T. Massie, D. P. Edwards, J. M. Flaud, A. Perrin, C. CamyPeyret, V. Dana, J. Y. Mandin, J. Schroeder, A. McCann, R. R. Gamache, R. B. Wattson, K. Yoshino, K. V. Chance, K. W. Jucks, L. R. Brown, V. Nemtchinov, and P. Varanasi, "The HITRAN Molecular Spectroscopic Database and HAWKS (HITRAN Atmospheric Workstation): 1996 edition," *Journal of Quantitative Spectroscopy and Radiative Transfer*, 60(5):665–710 (1998).

[8] L. S. Rothman, C. Camy-Peyret, J.-M. Flaud, R. R. Gamache, D. Goorvitch, A. Goldman, R. L. Hawkins, J. Schroeder, J. E. A. Selby, and R. B. Wattson, "HITEMP, the

High-Temperature Molecular Spectroscopic Database," *Journal of Quantitative Spectroscopy and Radiative Transfer*. In preparation.

[9] B. L. Upschulte and M. G. Allen, "Diode Laser Measurements of Line Strengths and Self-Broadening Parameters of Water Vapor between 300 and 1000 K near 1.3 μm," *Journal of Quantitative Spectroscopy and Radiative Transfer*, 59(6):653–670 (1998).

[10] V. Nagali, S. I. Chou, D. S. Baer, R. K. Hanson, and J. Segall, "Tunable Diode-Laser Absorption Measurements of Methane at Elevated Temperatures," *Applied Optics*, 35(21):4026–4032 (1996).

[11] Q. Kou, G. Guelachvili, M. Abbouti Temsamani, and M. Herman, "The Absorption Spectrum of C_2H_2 Around $\nu_1 + \nu_3$: Energy Standards in the 1.5 μm Region and Vibrational Clustering," *Canadian Journal of Physics*, 72(11–12):1241–1250 (1994).

[12] M. Herman, A. Campargue, M. I. El Idrissi, and J. Vander Auwera, "Vibrational Spectroscopic Database on Acetylene, $\tilde{X}^1\Sigma_g^+$ ($^{12}C_2H_2$, $^{12}C_2D_2$, and $^{13}C_2H_2$)," *Journal of Physical and Chemical Reference Data*, 32(3):921–1361 (2003).

[13] S. R. Tieszen, T. J. O'Hern, R. W. Schefer, E. J. Weckman, and T. K. Blanchat, "Experimental Study of the Flow Field In and Around a One Meter Diameter Methane Fire," *Combustion and Flame*, 129(4):378–391 (2002).

[14] A. L. Brown and T. K. Blanchat, "A Validation Quality Heat Flux Dataset for Large Pool Fires," *Proceedings of the 2003 ASME Summer Heat Transfer Conference*, HT2003-40249, ASME, New York, NY, 2003.

[15] "Material Safety Data Sheet: JP-8 Aviation Turbine Fuel," Phillips Petroleum Company, Bartlesville, OK, June 1989.

[16] C. R. Shaddix, S. W. Allendorf, G. L. Hubbard, D. K. Ottesen, and L. A. Gritzo, "Diode Laser Diagnostics for Gas Species and Soot in Large Pool Fires: LDRD Project Final Report," Sandia National Laboratories Report No. SAND2001–8383, June 2001.

[17] C. R. Shaddix, Á. B. Palotás, C. M. Megaridis, M. Y. Choi, and N. Y. C. Yang, "Soot Graphitic Order in Laminar Diffusion Flames and a Large-Scale JP-8 Pool Fire," *Combustion and Flame*, (2003). submitted.

[18] J. O. Hinze, *Turbulence*, second edition, McGraw-Hill, New York, NY, 1975.

[19] A. M. Obukhov, "On the Influence of Archimedean Forces on the Structure of the Temperature Field in Turbulent Flow," *The Reports of the USSR Academy of Sciences: Geophysics*, 125(6):1246–1248 (1959).

[20] R. Bolgiano Jr., "Turbulent Spectra in a Stably Stratified Atmosphere," *Journal of Geophysical Research*, 64(12):2226–2229 (1959).

[21] A. C. Eckbreth, *Laser Diagnostics for Combustion Temperature and Species*, second edition, Gordon and Breach Publishers, Amsterdam, 1996.

[22] T. Shimanouchi, *Tables of Molecular Vibrational Frequencies: Consolidated Volume I*, National Bureau of Standards, Washington, DC, 1972.

Appendix A: Temperature Dependence of Spectral Line Strength

The population of energy levels in the molecule is described by the Boltzmann distribution. The number of molecules populating a given vibrational-rotational level is given by [21]:

$$N_{v,J} \propto \frac{N}{Q_{vib}\,Q_{rot}} \exp\left[\frac{-E_{v,J}hc}{kT}\right] \tag{A.1}$$

For an absorption line, the line strength is proportional to the number of molecules in the lower state minus the number of molecules in the higher state.

$$S_i \propto N''_{v,J} - N'_{v,J} \propto \frac{N}{Q_{vib}\,Q_{rot}} \exp\left(\frac{-E''_{v,J}hc}{kT}\right)\left[1 - \exp\left(\frac{-\nu_i hc}{kT}\right)\right] \tag{A.2}$$

where $\nu_i = E'_{v,J} - E''_{v,J}$ is the energy of the transition. The temperature dependence of the line strength is thus given by

$$\sigma(T) = \frac{S_i(T)}{S_i(T_0)} = \frac{T_0}{T}\frac{Q(T_0)}{Q(T)} \exp\left[\frac{-E''_{v,J}hc}{k}\left(\frac{1}{T} - \frac{1}{T_0}\right)\right]\frac{1 - e^{-\nu_i hc/kT}}{1 - e^{-\nu_i hc/kT_0}} \tag{A.3}$$

where $Q(T) = Q_{vib}(T)\,Q_{rot}(T)$ is the product of the partition functions.

The vibrational partition function is given on p. 509 of Herzberg [6]:

$$Q_{vib} = \sum_i (1 - e^{-\omega_i hc/kT})^{-d_i} \tag{A.4}$$

The ω_i's in this equation can be obtained from Shimanouchi [22], while the degeneracies d_i are given on p. 119 and p. 121 of Herzberg [6]. For convenience, these parameters are summarized in Table A.1 for the molecules of interest.

The rotational partition function depends on the type of molecule. Acetylene is a linear molecule, which has the following partition function.

$$Q_{rot} = \frac{kT}{\sigma hcB} \tag{A.5}$$

Methane is a spherical top molecule, which has

$$Q_{rot} = \frac{1}{\sigma}\sqrt{\frac{\pi}{B^3}\left(\frac{kT}{hc}\right)^3} \tag{A.6}$$

for a partition function. These forms of the partition function are asymptotic approximations that are valid for $B/T \ll 1$. The rotational parameters for the two molecules of interest are shown in Table A.2. Both the rotational constant B and the symmetry parameter σ are given by Herzberg [6].

Table A.1. Molecular vibrational parameters.

Acetylene

Species	i	ω_i (cm^{-1})	d_i
Σ_g^+	1	3374	1
Σ_g^+	2	1974	1
Σ_u^+	3	3289	1
Π_g	4	612	2
Π_u	5	730	2

Methane

Species	i	ω_i (cm^{-1})	d_i
A_1	1	2917	1
E	2	1534	2
F_2	3	3019	3
F_2	4	1306	3

Table A.2. Molecular rotational parameters.

Molecule	Type	Symmetry	σ	B (cm^{-1})
C_2H_2	Linear	$D_{\infty h}$	2	1.17664
CH_4	Spherical top	T_d	12	5.241035

For acetylene, the lower energy level is calculated using from $E''_{v,J} = B_v J(J+1) + D_v J^2(J+1)^2 + H_v J^3(J+1)^3$ with the parameters $B_v = 1.17664632$, $D_v = 1.62710\times10^{-6}$, and $H_v = 1.6\times10^{-12}$ [11]. The line we are measuring is at 6495.9 cm^{-1}, which was identified by Kou et al. [11] as the P(23) line. Thus, $E''_{v,23} = 650.0048$.

The methane line used is a combination of six closely-spaced lines around 6077 cm^{-1}. Thus, the total line strength is the sum of the individual line strengths, i.e. $S(T) = \sum_i S_i(T)$. The values of the relevant energy levels were calculated by Nagali et al. [10]. These values are reproduced in Table A.3 below.

Table A.3. Spectroscopic parameters for methane at 296 K.

Line	ν_i (cm^{-1})	$S_i(T_0)$	$E''_{v,J}$ (cm^{-1})
1	6076.928	1.119	219.9135
2	6076.935	1.924	219.9368
3	6076.954	3.010	219.9199
4	6077.028	1.770	219.9413
5	6077.046	1.848	219.9150
6	6077.063	2.980	219.9452

Distribution

1 Philip J. Smith
Dept. of Chemical and Fuels Engineering
3290 Merrill Engineering Building
50 South Central Campus Drive
The University of Utah
Salt Lake City, UT 84112-9203

1 Jennifer Spinti
Dept. of Chemical and Fuels Engineering
3290 Merrill Engineering Building
50 South Central Campus Drive
The University of Utah
Salt Lake City, UT 84112-9203

1 Elizabeth J. Weckman
Dept. of Mechanical Engineering
University of Waterloo
Waterloo, Ontario
N2L 3G1
Canada

Sandia Distribution

1	MS 9054	W. J. McLean, 8300
1	MS 9054	D. R. Hardesty, 8360
1	MS 9053	J. O. Keller, 8367
1	MS 9052	L. G. Blevins, 8367
1	MS 9052	J. J. Murphy, 8367
5	MS 9052	C. R. Shaddix, 8367
1	MS 9052	T. C. Williams, 8367
1	MS 9051	A. Kerstein, 8351
1	MS 9052	R. W. Schefer, 8367
1	MS 1146	T. K. Blanchat, 9132
1	MS 1135	A. L. Brown, 9132
1	MS 1135	J. C. Hewson, 9132
1	MS 1135	K. A. Jensen, 9132
1	MS 1135	J. M. Suo-Anttila, 9132
1	MS 1135	S. R. Tieszen, 9132
1	MS 0834	S. P. Kearney, 9112
1	MS 0834	T. J. O'Hern, 9112
1	MS 0821	L. A. Gritzo, 9132

3	MS 9018	Central Technical Files, 8945-1
1	MS 0899	Technical Library, 9616
1	MS 9021	Classification Office, 8511 for Technical Library, MS 0899, 9616
		DOE / OSTI via URL